ORNL/TM--8059

DE82 013738

ORNL/TM-8059
Dist. Category UC-77

Contract No. W-7405-eng-26

CHEMICAL TECHNOLOGY DIVISION

THE INTERACTION OF PALLADIUM, THE RARE EARTHS, AND SILVER WITH SILICON CARBIDE IN HTGR FUEL PARTICLES

R. L. Pearson
R. J. Lauf*
T. B. Lindemer

*Metals and Ceramics Division

Date Published - April 1982

OAK RIDGE NATIONAL LABORATORY
Oak Ridge, Tennessee 37830
operated by
UNION CARBIDE CORPORATION
for the
DEPARTMENT OF ENERGY

THE INTERACTION OF PALLADIUM, THE RARE EARTHS, AND SILVER WITH SILICON CARBIDE IN HTGR FUEL PARTICLES

R. L. Pearson
R. J. Lauf
T. B. Lindemer

ABSTRACT

The interactions of the simulated fission products palladium, rare earths, and silver with the silicon carbide (SIC) Triso-coated, high-temperature, gas-cooled reactor (HTGR) particles were investigated out-of-reactor in the temperature range 1500 to 1780 K. Both palladium and the rare earths interact in proportion to time (rather than the square root of time) up to 8600 h (0.98 year), the time limit of the study. Grain-boundary mechanisms are suggested. Effects of the SiC microstructure on the palladium reaction rate were minimal in comparison to the temperature effects. Silver interactions with SiC were observed, but could not be quantified.

In a second set of experiments, the addition of silicon to carbide-containing kernels resulted in retention of U-Pd-Si-C compounds in the kernel. These prevented the reaction of palladium with SiC at temperatures of 1670 to 1920 K as long as rare-earth carbides were not present.

---

1. INTRODUCTION

During the past several years, the Oak Ridge National Laboratory (ORNL) has published several reports relating to fission product interaction with the SiC layer in HTGR fuel particles.[1-6] Of the many fission products formed during irradiation, the noble metal palladium and the rare earths interact significantly with SiC. Silver, which diffuses through SiC, will also react with it in some cases.[5-7] Reactions between fission products and SiC can decrease the thickness of the SiC layer and, ultimately, may result in fission-product release. The decrease is equivalent to the depth of the interaction zone and is termed "thinning"

of the SiC. Core design studies conducted at General Atomic (GA) have shown that fuel failures and fission product releases associated with reactions of fission products with SiC in Triso-coated fissile fuels may limit the allowable range of core outlet temperatures for an HTGR. Early core design studies were based on data analysis indicating that the decrease in SiC thickness was linear with time.[1] This assumption has recently been questioned, and a reanalysis by GA of some of the SiC thinning data suggested that the change in SiC thickness might be proportional to the square root of time rather than directly proportional to time.[8]

This report investigates the time dependence of fission product–SiC interactions and presents ways the silicon carbide thinning rate may be reduced.

Early SiC coating development work[9] showed that varying deposition parameters can significantly affect the coating microstucture. Later work[10] identified microstructural defects at the submicron level and further clarified the relation between microstructural details and coating process variables. Transmission electron microscopy (TEM) was particularly useful in characterizing the deposited SiC. For this reason, TEM and associated microanalytical techniques were also used to examine the SiC on particles doped with fission product elements and subsequently annealed in a thermal gradient.

2. TIME DEPENDENCE OF FISSION PRODUCT–SiC INTERACTIONS

2.1 Materials and Heat Treatment

Batches of simulated Triso-coated particles containing LaC_2, NdC_2, UO_2 plus palladium, or UO_2 plus silver kernels were used in long-term, high-temperature studies to clarify the time dependence of the fission product–SiC interactions. The characteristics of each batch are listed in Table 1.

The SiC coatings of all the palladium-containing particles were contaminated with palladium. Interestingly, this palladium contamination disappeared by the time the 995-h samples were removed and was only

Table 1. Summary of experimental SiC coating runs

Batch[a]	Run	Deposition temperature (°C)	Coating[b] rate (μm/min)	SiC density (mg/m^3)	SiC thickness (μm)
OR-2667	393	1550	0.58		28
OR-2668	394	1550	1.20		30
Pd-1	499	1500	0.44	3.208	22
Pd-2	500	1550	0.39		20
Pd-6	489	1550	0.78		35
Pd-8	493	1700	0.79		32
Pd-10	498	1550	1.03		41
Pd-11	496	1650	0.97	3.207	33
Pd-12	497	1700	1.29		31
Ag-1	508	1500	0.40		24
Ag-2	511	1550	0.39		24
Ag-10	512	1550	1.19		36

[a]Batch designations are as follows: Ag = (UO_2 + 1.26 wt % Ag) kernels, Pd = (UO_2 + 0.54 wt % Pd) kernels, OR-2667 = LaC_2 kernel, and OR-2668 = NdC_2 kernel. The inner Low Temperature Isotopic (iLTI) coatings were chlorine leached at 1500°C for 18 h to insure that chlorine contamination of the buffer layer did not occur. One iLTI-coated batch of palladium-containing kernels was used for the SiC coating runs; a similar procedure was used for the silver-containing kernel.

[b]All coatings were deposited in a 2.5-cm diameter coater.

partially present in the 485-h samples (Sect. 2.3). The contamination first disappeared from the outside of the SiC layer and at a rate that was apparently much faster than the rate given by Eq. (2), Sect. 2.3.

Single graphite wafers containing 20 particles of batches OR-2667 or OR-2668 and several graphite wafers each containing 20 particles of batches Pd-1, Pd-2, Ag-2, and Ag-10 were formed and mounted for heat treatment at 1773 K in a temperature gradient across the wafer of 27.8 K/mm. Each wafer, therefore, contained Triso-coated particles heat-treated at temperatures ranging from ~1500 to 1773 K. The technique used to prepare and heat treat particles in this manner has been published previously.[11]

2.2 Time Dependence of Rare-Earth Interactions with SiC

The wafers filled with Triso-coated particles containing LaC_2 and NdC_2 kernels were removed from the furnace after treatment for 485, 995, 2057, 4016, 6005, and 8600 h, radiographed each time, then returned to the furnace for further heat treatment. From the radiographs it was possible to determine the amount of SiC thinning with an optical microscope, because a sharp interface could be seen in the SiC at the point of maximum rare-earth penetation. The results are illustrated in Fig. 1. As shown in an earlier study,[1] the thinning rate of SiC in contact with NdC_2 or LaC_2 was dependent on time, rather than the square root of time. The thinning rate found from the experiments of this study falls within the 95% confidence limits of the earlier report.[1,6]

2.3 Time Dependence of Palladium Interactions with SiC

2.3.1 Procedure

Silicon carbide thinning could not be determined from radiographs of the Triso-coated particles containing either palladium or silver, since a sharp fission product—SiC interface did not form. Instead, separate nodules containing palladium and areas where the SiC had been replaced by silver were dispersed randomly in the grain boundaries of the SiC layer.

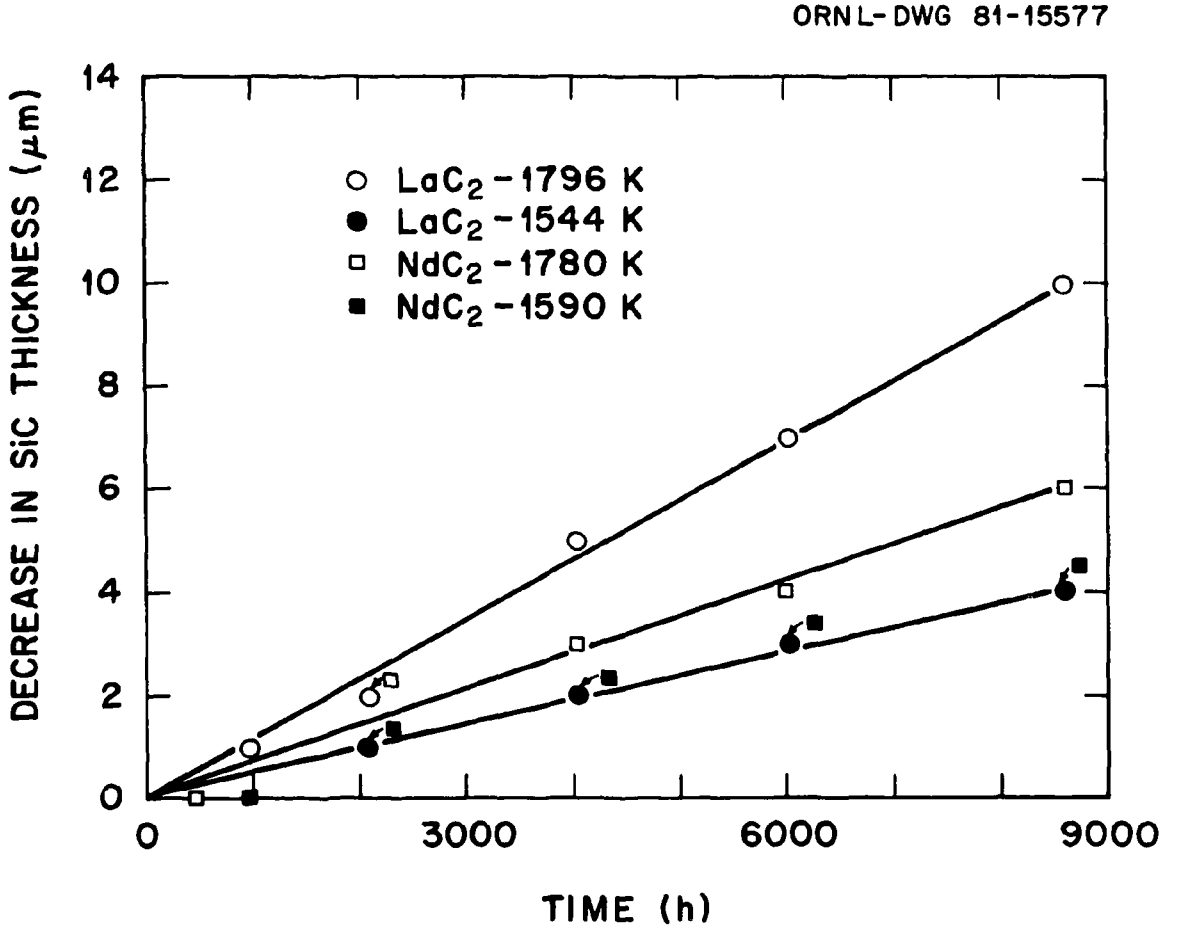

Fig. 1. The thinning of the SiC layer by NdC_2 or LaC_2 versus time.

One sample from each set of wafers was removed from the furnace after heat treatments of 485, 995, and 4016 h; these were mounted and polished to the midplane of the particles. A fourth wafer, which had previously been heat-treated for 2000 h, was available from the experiments reported in ORNL/TM-7393.[5] Because of the small size of some of the palladium nodules (<1 μm), the maximum depth of palladium penetration into the SiC could be detected best with a scanning electron microscope (SEM). We used an ISI Model Super-IIIA SEM, with a Robinson backscattered electron detector and a Kevex x-ray spectrometer. All of the data gathered are listed in the Appendix.

2.3.2 Data analysis

These data were analyzed by least-square techniques. The data were fitted to the Arrhenius equation in the form

$$\ln (x/t^n) = \ln A - Q/RT \ , \qquad (1)$$

where x is the maximum palladium penetration (μm) into the SiC, t is time (s), A is the preexponential coefficient (μm/s), Q is the activation energy (kJ/mol), R is the gas constant (8.314 J mol^{-1} K^{-1}), and T is temperature (K). Since the examination technique was destructive, the value of n could not be determined by plotting the x-t data from a single particle, as was done in Fig. 1. Instead, a computer program iterative procedure was used in which successive values of n were assumed, with $0.25 \leq n \leq 1.75$, in increments of 0.01. At each value of n, the coefficients A and Q in Eq. (1) were determined from the x-t-T data (see Appendix, Table A-1) by standard least-squares techniques. Then, the sum of the square of the residuals, i.e., the term $\sum_{i=1}^{N} [y_i(\text{experimental}) - y_i(\text{fitted})]^2$, was determined, in which $y = \ln (x/t^n)$. The best-fit value of n was assumed to be that when the sum was a minimum. All the data could be fit best by using n = 0.80 (Fig. 2). This was a sensitive method for determining the value of n because the minimum value of the sum was 0.40 of the maximum values of the sum (the maxima occurring at n = 0.25 and 1.75).

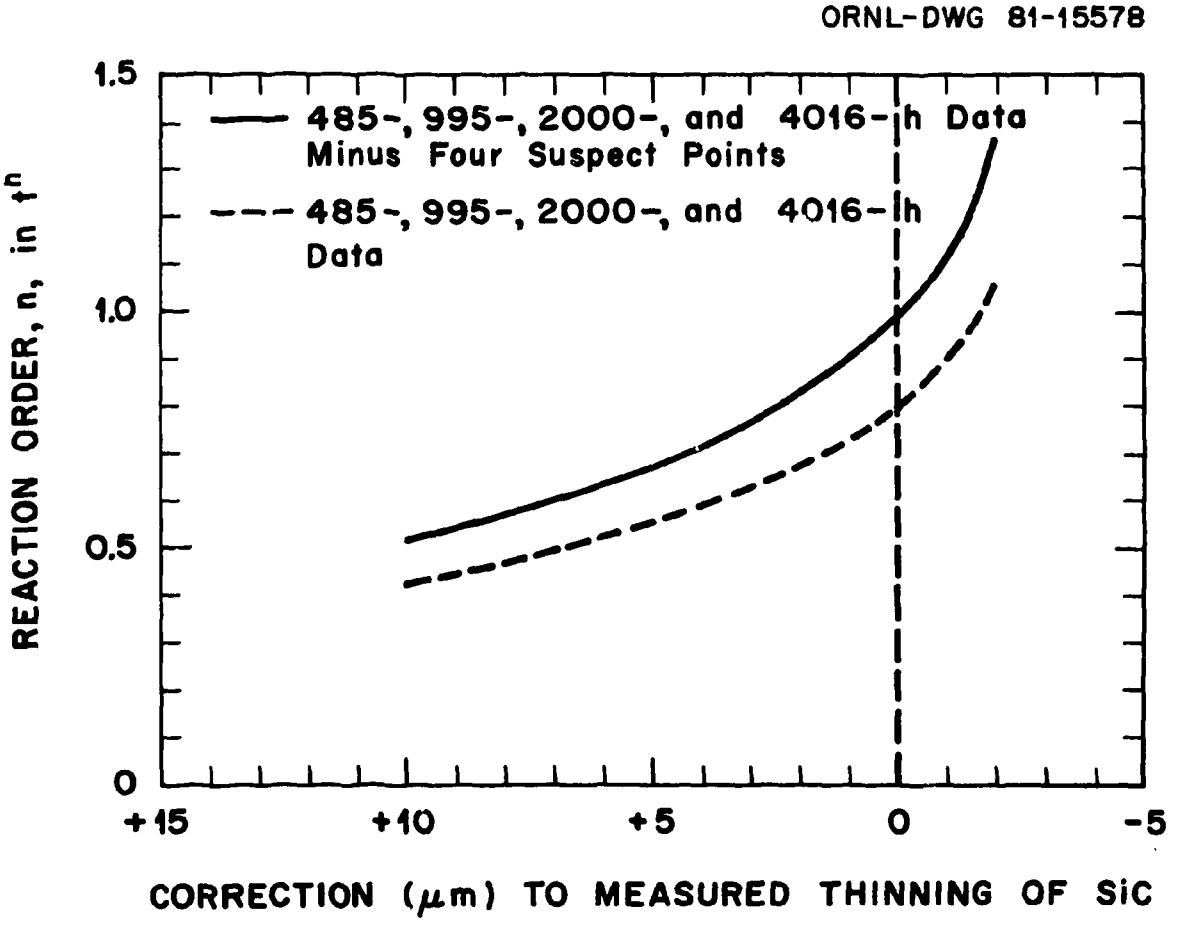

Fig. 2. The least-squares-fitted values of n in t^n versus the correction to the measured penetration of SiC by palladium from $1670 \leq T \leq 1920$ K (see Sect. 2.3).

Further analysis of the data indicated that a linear time dependence (n = 1), can be obtained by subtracting 1.7 μm from each penetration measurement. This is not unreasonable, because SEM photographs of the inner surface of typical SiC layers show the first 1-2 μm of the SiC to have a spongy structure which may easily be permeated by fission products.[12] Therefore, the exact location of the SiC-iLTI interface is difficult to pinpoint. The data from each heat treatment follow a reasonable pattern except for points 5 through 8 of the 485-h heat treatment. These points are suspect because of palladium contamination of the SiC layer during deposition, rather than Pd-SiC interaction during heat treatment. When these four points, or all 485-h data are excluded, the remaining penetration data could be fit best by using the reaction order n = 0.99 (Fig. 2), without correcting the location of the SiC-iLTI interface. This is essentially a linear time dependence of palladium interaction with SiC. In either case, to obtain a square-root time dependence, 6.7 and 11.2 μm, respectively, must be added to the penetration measurements in Fig. 2. Such a large correction cannot be justified.

The linear thinning rate and 95% confidence limits calculated from the data (Appendix, Table A-1), excluding the four suspect points at 485-h, are plotted versus reciprocal temperature in Fig. 3. Here the Arrhenius equation is

$$x/t = 0.0319 \exp(-128{,}000/RT) \ . \qquad (2)$$

Plotted on the same figure are the thinning rate and 95% confidence limits calculated previously for Pd-SiC interaction data measured in irradiated particles with the optical microscope.[4,6] The activation energies for the two data sets are nearly the same, but the rate calculated from data measured by SEM is approximately five times greater than the rate calculated from data measured by optical microscope. This is not surprising, since the SEM can detect palladium penetration further into the SiC layer, as well as under the surface of the SiC. The 95% confidence limits of the data obtained using the SEM are also much narrower.

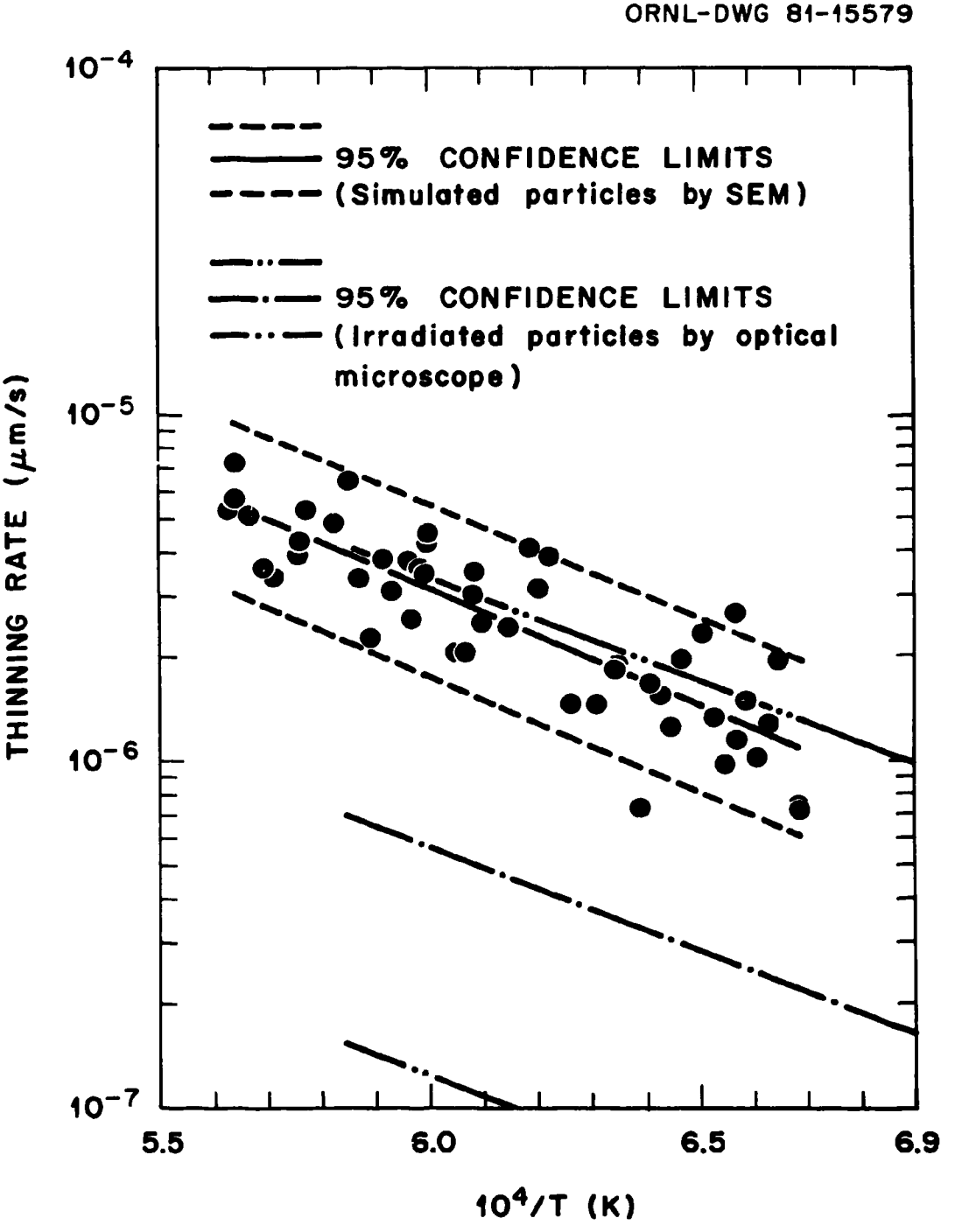

Fig. 3. The thinning rate versus reciprocal temperature for the interaction of palladium with SiC.

2.4 Silver Interactions with SiC

No silver penetration into the SiC layer, other than an occasional large nodule where the SiC had been completely replaced by silver, could be detected by SEM in the heat-treated, Triso-coated, silver-containing particles. Consequently, no time–temperature dependence of silver interactions with SiC could be determined. Further discussion follows in Sect. 3.2.

3. MECHANISMS OF NOBLE METAL ATTACK

3.1 Palladium

Twelve batches of Triso-coated, palladium-doped particles were examined by optical microscopy after a 2000-h anneal in the thermal gradient furnace; the results were published previously.[5] Seven of these wafers were reexamined with the SEM, and the data are given in the Appendix, Table A-2. It was assumed that the penetration of palladium into the SiC is governed by an Arrhenius equation:

$$x = A_1 \exp(-Q/RT) , \qquad (3)$$

where A_1 is the preexponential constant (μm).

A plot of the data for batch Pd-6 (Table 1) is shown in Fig. 4. This batch yielded the best agreement with an Arrhenius relationship; some batches gave one or more suspect data points. Table 2 gives the slope (-Q/R) of the Arrhenius plot for each batch examined by SEM after 2000 h. Values of Q and the standard deviation, s, are also given for each batch.

Figure 5 shows a plot of the apparent activation energy for noble metal attack versus the SiC deposition temperature. Several observations can be made:

1. Typical values of the activation energy for carbon diffusion in a liquid metal are generally much less than the values of Q reported here. This suggests that carbon diffusion in the noble metal nodule is probably not the rate-limiting process.

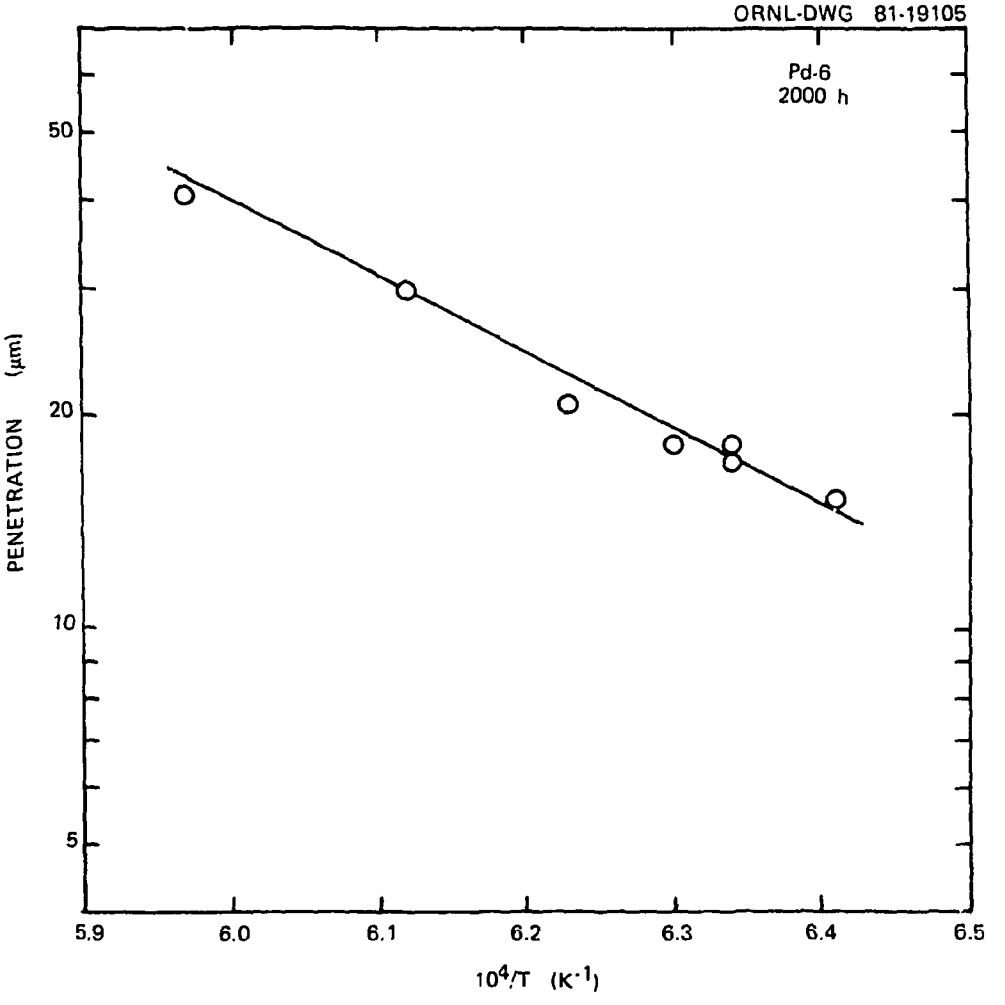

Fig. 4. Arrhenius plot for palladium attack of SiC during the thermal gradient annealing test.

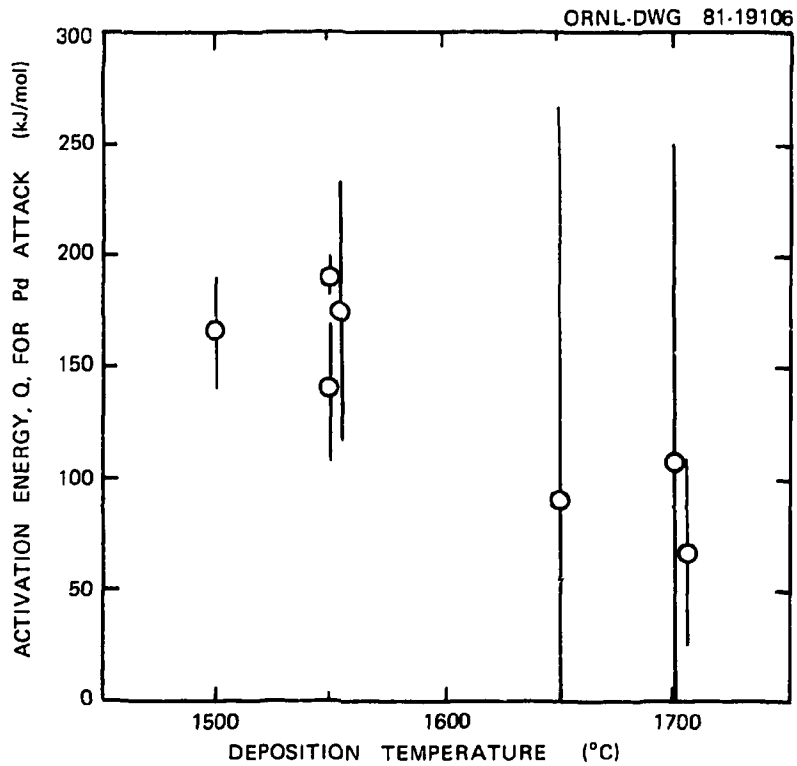

Fig. 5. Apparent activation energy, Q, for palladium attack of SiC versus deposition temperature.

Table 2. Activation energies for palladium attack

Batch	Slope	Q (kJ/mol)		s (kJ/mol)
Pd-1	-0.20×10^5	166	±	25
Pd-2	-0.17×10^5	141	±	33
Pd-6	-0.23×10^5	191	±	8
Pd-8	-0.13×10^5	108	±	141
Pd-10	-0.21×10^5	175	±	58
Pd-11	-0.11×10^5	91	±	175
Pd-12	-0.08×10^5	67	±	42

2. Despite some uncertainty in the data, there appears to be a relationship between the activation energy and the SiC deposition temperature. This suggests that microstructural features play a role. Since previous work[10] showed that high deposition temperatures tend to favor large, columnar grains, it is possible that grain boundary transport is the controlling process.

3. The activation energy for bulk (vacancy-assisted) diffusion in SiC would be at least a factor of four greater than the observed values of Q.[13] This is further evidence suggesting transport along grain boundaries or some other path of enhanced mobility.

Transmission electron microscopy (TEM) showed very small ($\leq$1 μm) nodules of a noble metal compound occurring along SiC grain boundaries (Fig. 6). There does not appear to be significant restructuring behind the nodules, which suggests that the nodules move by dissolving SiC at the leading edge and forming SiC at the trailing edge. As shown in Fig. 7, the newly formed SiC could grow directly on the original material, maintaining the same orientation and leaving the microstructure relatively unaffected. The presence of other fission product elements in an operating fuel particle could, of course, inhibit the repair process and lead to local corrosion and thinning of the SiC.

Energy-dispersive x-ray analysis (EDX) of the nodules in Fig. 6 indicated the presence of Pd, Rh, U, and Si. This is consistent with

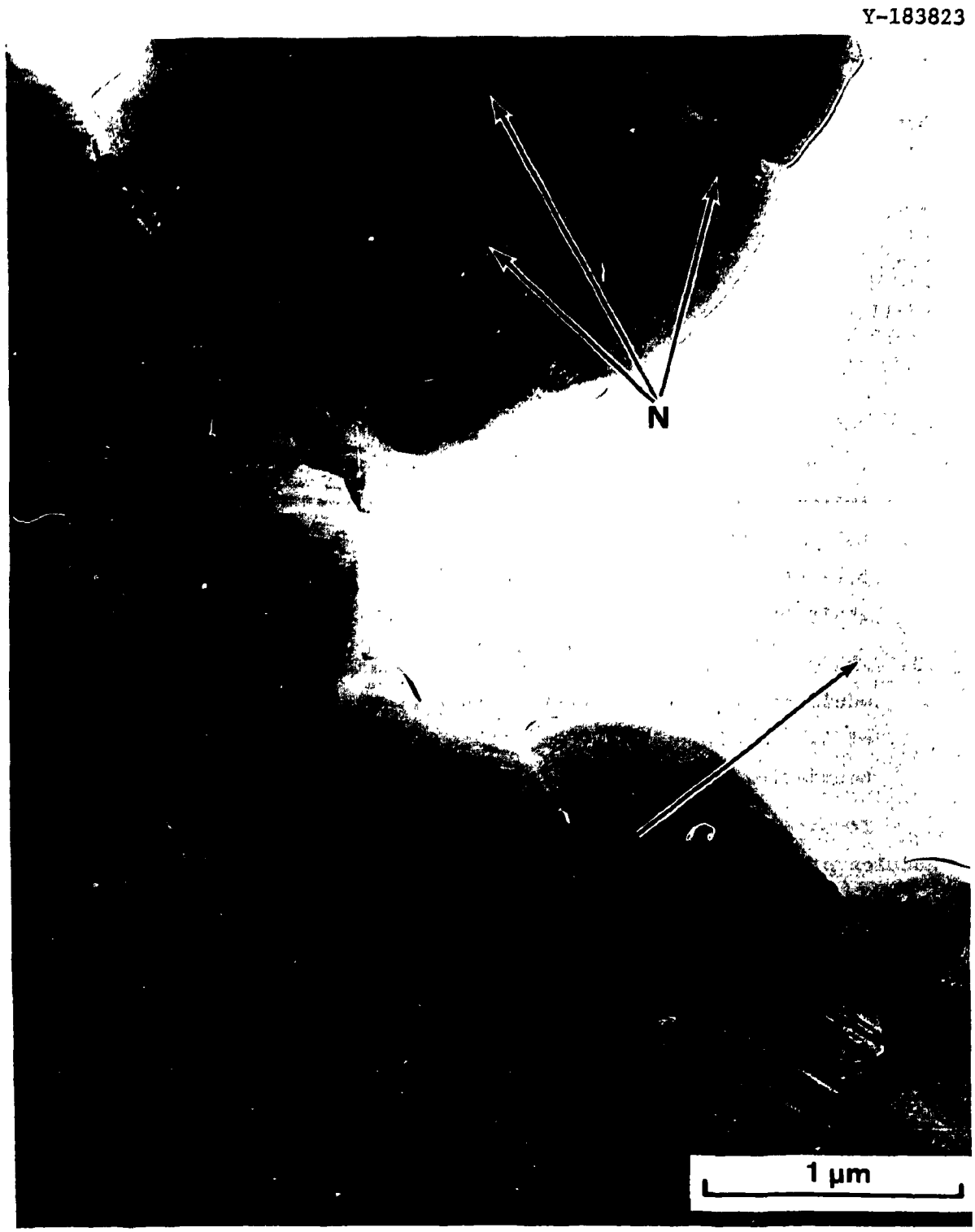

Fig. 6. Transmission electron microscope (TEM) photograph of noble metal nodules (N) in SiC coating after a UC_2-Mo-Ru-Rh-Pd particle has been annealed in the thermal gradient furnace for 260 h at a temperature of 1597°C. Arrow indicates radial outward direction of the SiC coating.

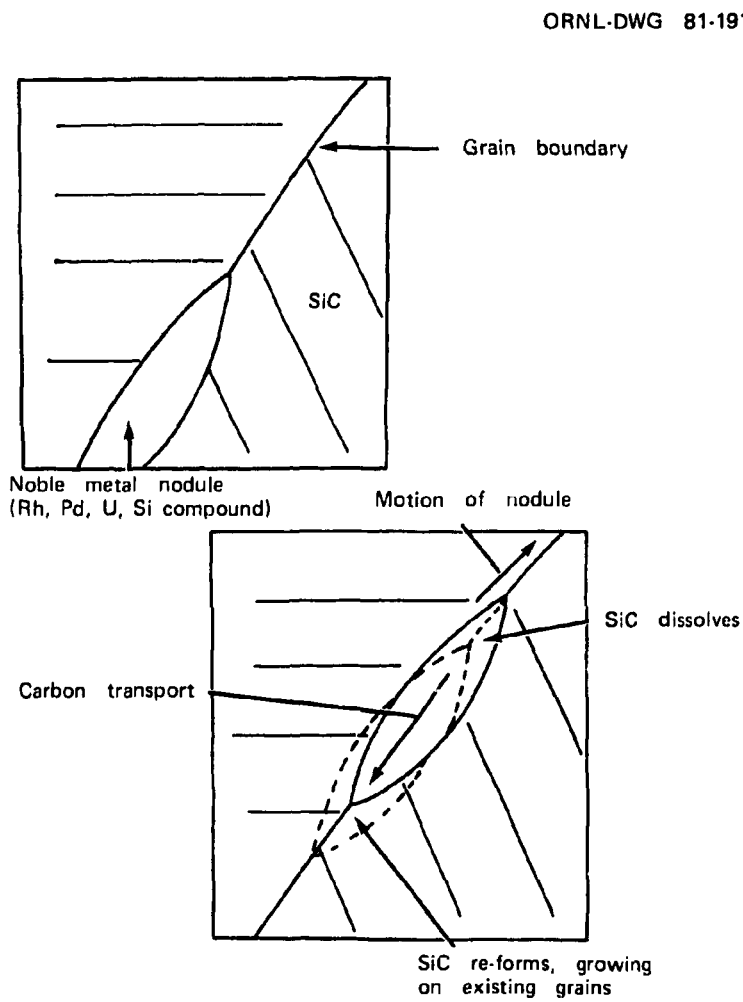

Fig. 7. Schematic illustration of possible noble metal transport process in SiC coating.

electron microprobe results, except that prior observations were unable to identify rhodium conclusively because of overlapping Kα lines of palladium and rhodium. Distinct Lα lines for palladium and rhodium were seen when EDX was done in the TEM.

3.2 Silver

Previous work[5,6] showed that high concentrations of silver will attack SiC, displaying Arrhenius behavior with about the same activation energy as palladium does in its attack. At the low concentrations typical of operating fuel particles, silver can escape from the particle, apparently by diffusing through intact SiC. The TEM examination of several particles from batch Ag-1 (Table 1) after 2000 h of annealing revealed no microstructural changes on either the hot or cold sides of the particles. No second-phase nodules were detected, nor were there any obvious grain boundary films. Figure 8 shows a typical coating from this wafer. A small circumferential string of voids was observed in one coating from this wafer. There was no evidence of silver accumulation in the voids, although microanalysis in the scanning-transmission (STEM) mode should be done to verify this. Similarly, the small (2.0 nm) probe size in the STEM mode might reveal small amounts of silver along grain boundaries or other defects. More work is planned in this area.

4. METHODS FOR MINIMIZING FISSION-PRODUCT ATTACK OF SiC

If SiC thinning could be reduced or eliminated, there would be more latitude for the design of an HTGR with higher core outlet temperatures. Both palladium and rare earth interactions with SiC may be alleviated at practical HTGR temperatures, as discussed below.

4.1 Rare Earths

In an earlier study,[3] it was learned that the movement of rare earth fission products within Triso-coated particles was practically eliminated if the rare earths existed as oxides. This is accomplished through stoichiometric control of the kernel and has been demonstrated in-reactor.[2,3,14]

Y-183824

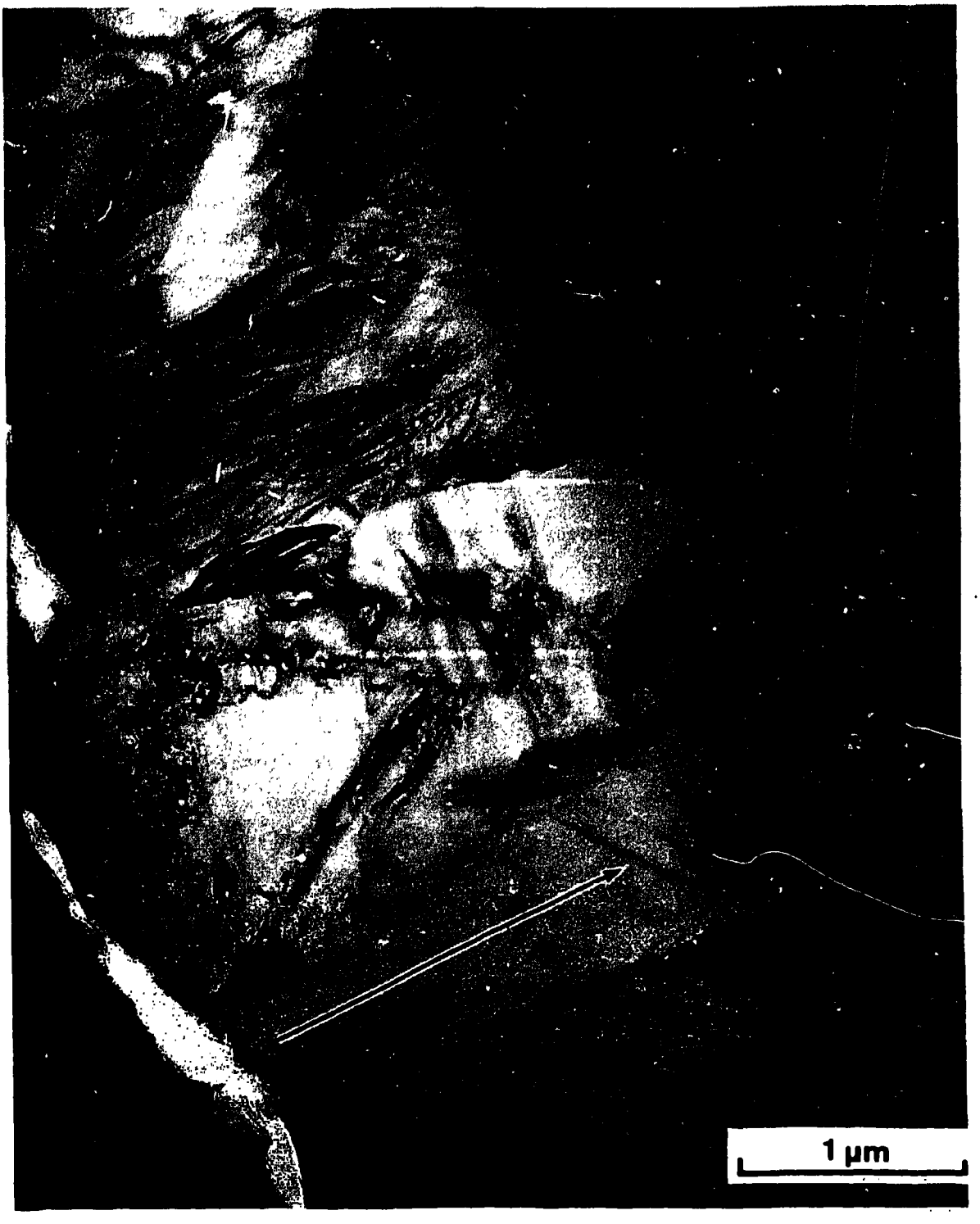

Fig. 8. Microstructure of SiC coating Ag-1, on UO_2 + Ag kernel, after 2000 h at ~1475°C. No second phases or grain boundary films could be seen. Arrow indicates radial outward direction of SiC coating.

4.2 Palladium

It may be possible to immobilize palladium in a carbide-containing kernel as a U-Pd-Si-C compound. A literature search for palladium-containing compounds not previously considered in the system of fuel, fission products, and SiC revealed MPd_2Si_2 and MRh_2Si_2, in which M represents yttrium and lanthanum through erbium of the lanthanide series.[15] Because of the chemical similarity of lanthanide and actinide compounds, UPd_2Si_2 was suggested. Previously, the most stable known palladium-containing compound was UPd_3, which was calculated to be the equilibrium form of palladium in carbide-containing HTGR fuels.[6] If UPd_2Si_2 were more stable than UPd_3 in the U-Pd-Si-C system, one might expect the reaction

$$0.67UPd_3 + 2SiC + 0.33UC_2 \not\rightleftharpoons UPd_2Si_2 + 2.67C \ .$$

To test this hypothesis, amounts of uranium, palladium, SiC, and UC_2 were arc melted and annealed. If the phase set on the left in the above reaction were stable, they should have been present in the sample. They were *not*, nor was UPd_2Si_2. Instead, metallography revealed at least two new U-Pd-Si-C compounds. These are, therefore, more stable than either UPd_3 or UPd_2Si_2, offering more hope of reducing the palladium chemical activity in the particle to less than that required for interaction with the SiC coating. The approximate melting points of several arc-melted U-Pd-Si-C samples were determined. One of the samples, with a U:Pd:Si:C molar ratio of 1:3:3:5, had a melting point >1950°C. This is much higher than the melting point of palladium or any other known palladium compounds. Palladium stabilization or gettering may, therefore, be possible by intentionally adding SiC to UC_2 or UO_2-UC_2 kernels; the UO_2-UC_2 kernel is favored (see discussion below).

Stabilization of palladium in the kernels of Triso-coated particles was investigated at $1670 \leq T \leq 1920$ K. Silicon and carbon were added to the kernel compositions of batches 2-1 and 2-3 of an earlier study.[16] The new kernel compositions and the kernel composition of particle batch OR-2773, which was used as a standard, are listed in Table 3. Batch OR-2773 simulates particles with kernels having 93% ^{235}U enrichment and

Table 3. Kernel compositions used for Pd-SiC interaction minimization studies

Batch[a]	UC_2	Mo	Ru	Rh	Pd	LaC_2	SiC	C	$\frac{Si}{Mo + Ru + Pd}$
					Kernel composition (wt %)				
OR-2773	77.0	12.5	6.0	1.4	0.9			1.9	
5-1	71.9	8.3	7.0		3.1		7.5	2.2	
5-5	71.7	7.2	6.0		2.7	6.0	12.9	3.7	
					Kernel composition (molar ratio)				
5-1	75	24	19		8		51	50	1
5-5	75	24	19		8	12	102	97	2

[a]The iLTI coating of OR-2773 was chlorine leached at 1500°C for 18 h to insure that chlorine contamination of the buffer layer did not occur. Batches 5-1 and 5-5 were not chlorine leached.

irradiation to 64% FIMA. Batches 5-1 and 5-5 (see ref. 17) simulate particles with kernels having 20% ^{235}U enrichment and 25% FIMA (13.75% ^{235}U; 11.25% ^{239}Pu). The amounts of molybdenum, ruthenium, and palladium added to the kernels of batches 5-1 and 5-5 were increased by a factor of four over those present in-reactor, to assure detection by EDX. Triso-coated particles of each batch were enclosed in graphite wafers and heated at a peak temperature of 1923 K (1650°C) for 165 h in a 27.8 K/mm temperature gradient. The general observations made in these experiments are summarized in Table 4 and given in full detail below.

The results of the heat treatment for batch OR-2773, the standard, are seen in the composite set of photographs comprising Fig. 9. In Fig. 9a, the as-produced particle exhibits little or no heavy metal at the iLTI-SiC interface. After heat treatment (Fig. 9b), there are heavy metals at the interface, and some have penetrated into the SiC layer. In Fig. 9c, which is a magnification of Fig. 9b, uranium, palladium, and rhodium were identified in the iLTI layer. At the iLTI-SiC interface, the two main elements were uranium and silicon. The nodules within the SiC layer contained uranium, palladium, and silicon. The nodules probably contained carbon also, but the x-ray dispersive unit was unable to identify it. The elements remaining in the kernel after heat treatment were ruthenium, molybdenum, and uranium.

The results of the heat treatment of batch 5-1, where SiC was added to the kernel, are seen in the composite set of photographs comprising Fig. 10. Very little heavy element movement can be detected even after heat treatment. Figure 10b, which is a magnified photograph of the iLTI-SiC interface of a heat-treated particle, appears very similar to Fig. 10a, an as-produced particle. Figure 10c is a magnification of the kernel-buffer interface. Within the buffer layer, there were only a few faint areas containing uranium, ruthenium, and silicon. All of the palladium was associated with uranium, silicon, ruthenium, and molybdenum within the kernel.

The results of the heat treatment of batch 5-5 are seen in the composite set of photographs comprising Fig. 11. Figures 11a, 11b, and 11c are photographs of the iLTI-SiC interface of the as-produced and heat-treated particles. When heat-treated, both palladium and lanthanum

Table 4. Location of elements in Triso-coated particles

Batch	Original kernel[a]	After 165 h at 1670 ≤ T ≤ 1920 K[b]			
		Kernel	Buffer layer	iLTI layer	SiC layer
OR-2773	UC_2 + Mo, Ru, Rh, Pd	U, Mo, Ru	Not determined	U, Pd, Rh	U, Pd, Si
5-1	UC_2 + Mo, Ru, Pd, SiC	U, Mo, Ru, Pd, Si	U, Ru, Si	None	None
5-5	UC_2 + Mo, Ru, Pd, LaC , SiC	U, Mo, Ru, Si	U, La	Pd, La	Pd, La, Si

[a] See Table 3.

[b] Elements detected by Robinson backscattered electron detector coupled with an x-ray energy-dispersive spectrometer.

Y-183149

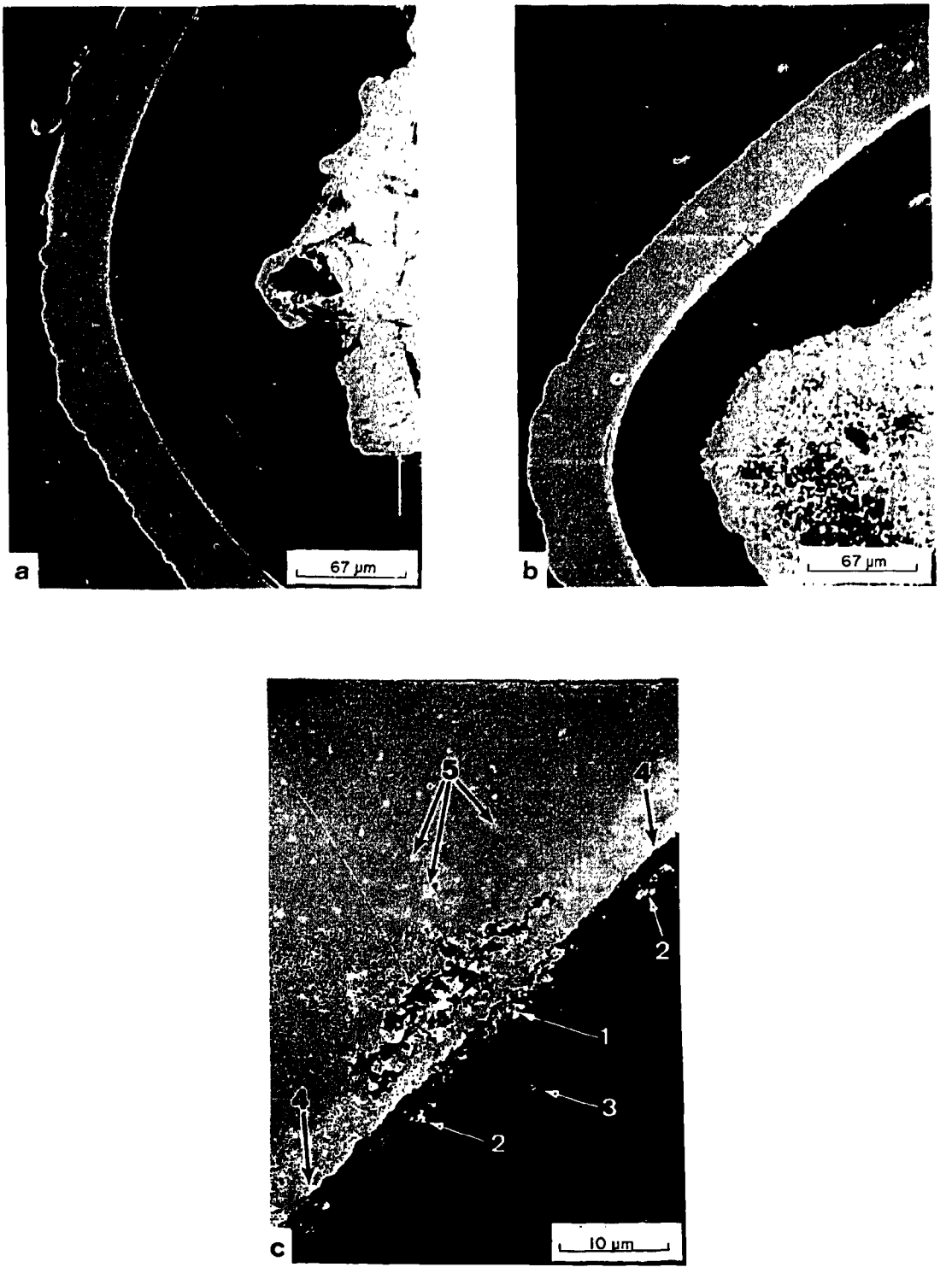

Fig. 9. Photographs of Triso-coated kernels of UC_2 containing Mo, Ru, Rh, and Pd (batch OR-2773). (a) As-produced particle, (b) particle heated at 1886 K for 165 h, (c) magnified iLTI-SiC interface of particle shown in (b). Legend: (1) Pd; (2) U-Pd; (3) U-Pd-Rh; (4) U-Si; (5) U-Pd-Si.

Y-183150

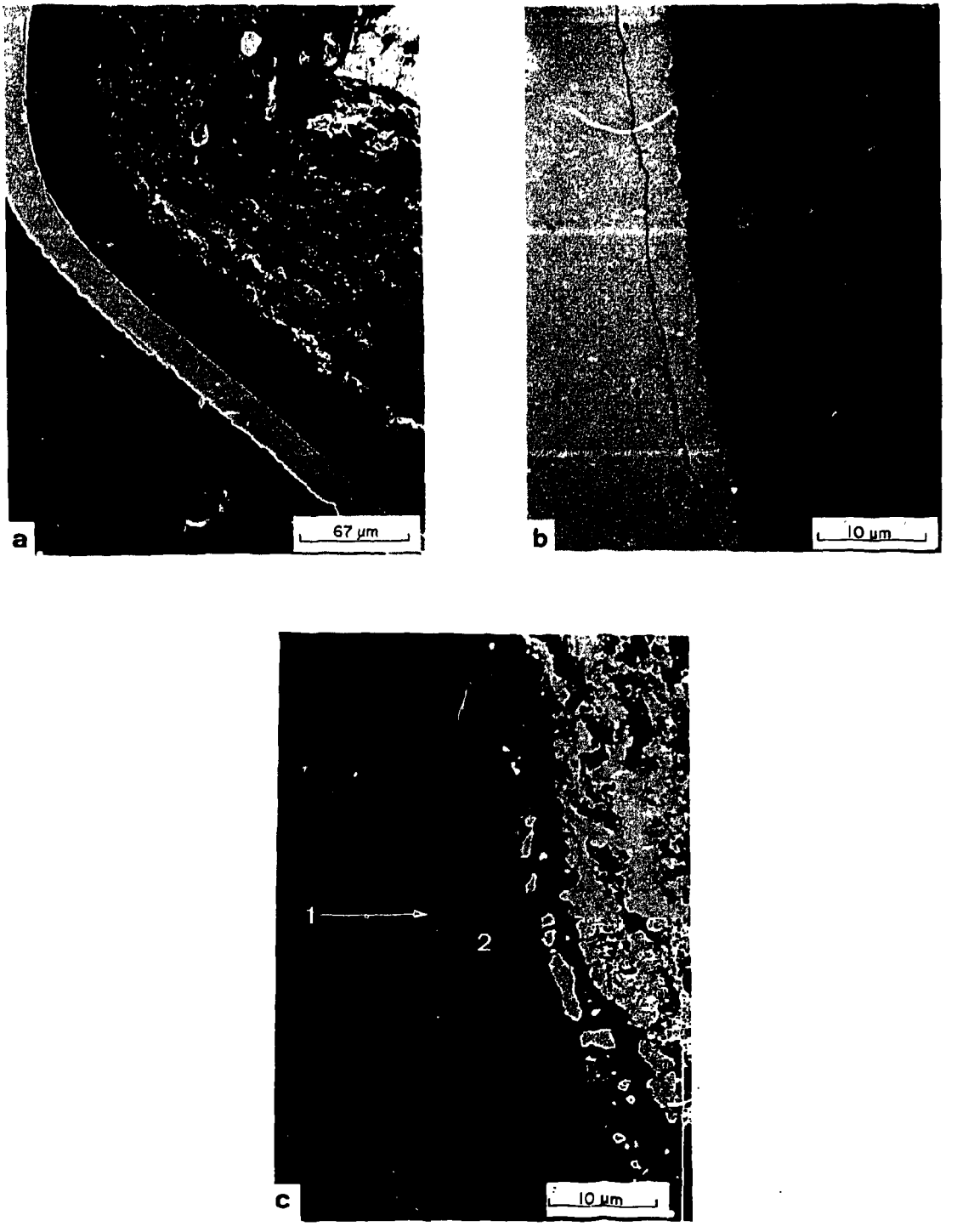

Fig. 10. Photographs of Triso-coated kernels of UC_2 containing Mo, Ru, Pd, and SiC (batch 5-1). (a) As-produced particle, (b) magnified iLTI-SiC interface heated at 1870 K for 165 h, particle in iLTI layer has Si-Mg in it. Probable source is furnace wall as iLTI was deposited. (c) Magnified kernel-buffer interface of particle shown in (b). Legend: (1) U-Si-Ru; (2) U-Si-Pd-Ru-Mo.

Y-183151

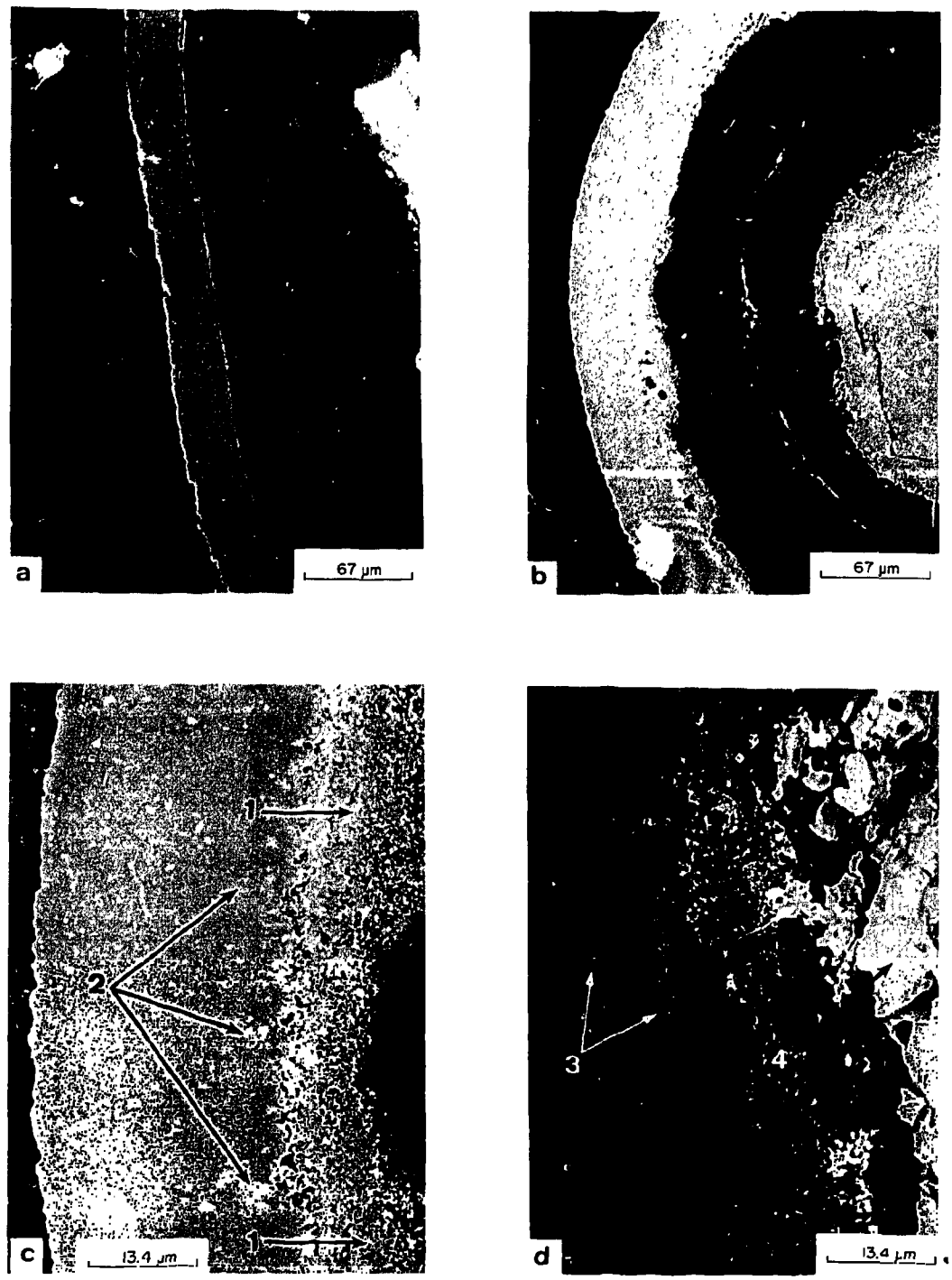

Fig. 11. Photographs of Triso-coated kernels of UC_2 containing Mo, Ru, Pd, LaC_2, and SiC (batch 5-5). (a) As-produced particle, (b) particle heated at 1886 K for 165 h, (c) magnified iLTI-SiC interface of particle shown in (b), (d) magnified kernel-buffer interface of particle shown in (b). Legend: (1) Pd-La; (2) Si-Pd-La; (3) U + La; (4) U + Si-Ru-Mo.

permeated the iLTI layer and accumulated at the iLTI-SiC interface (see Figs. 11b and 11c). The nodules within the SiC layer contained palladium, lanthanum, and silicon. In Fig. 11d, which is a magnification of the kernel–buffer layer interface, some uranium and lanthanum can be seen in the buffer layer. Uranium, rhenium, molybdenum, and silicon remained in the kernel.

Thus, the results seen in Figs. 9 and 10 indicate that, under the right conditions, the addition of SiC to the kernel can reduce or eliminate the attack of SiC coatings by palladium. It appears from Fig. 11, however, that the presence of lanthanide carbides is deleterious. This can be alleviated in-reactor by using UO_2-UC_2 kernels having the required UO_2 content.[2,14] Preliminary thermochemical calculations indicate that the U-Pd-Si-C compounds would be stable in these kernels and would result from irradiation of an initial UO_2-UC_2-SiC kernel fabricated from a UO_2-SiO_2-C mixture instead of the usual UO_2-C mixture.

4.3 Coating Optimization

Microstructural observations (Fig. 6) and kinetic considerations suggest that noble metal attack or transport involves the SiC grain boundaries almost exclusively. This implies that large, columnar grains with highly disordered boundaries would be undesirable from the standpoint of noble metal retention.

Large, columnar grains would provide a more direct diffusion path than would small, equiaxed grains having a more interlocking structure. This might explain the trend shown in Fig. 5.

The boundary between two heavily faulted SiC grains is probably much more disordered and is effectively "wider" than a boundary between two nearly perfect grains. Voids or gaps at grain boundaries or grain boundary junctions are probably also deleterious. This is consistent with observations that increasing the SiC coating rate tends to increase the palladium attack rate.[4,5]

In all cases, the microstructural effect is rather weak compared to the effect of annealing temperature or irradiation temperature. Furthermore, irradiation tends to cause numerous microstructural changes, such

as void formation and the elimination of some stacking faults. These changes might reduce the potential benefits of an optimum microstructure. The planned TEM examinations after irradiation of systematically varied SiC coatings will yield much needed information on this aspect.

5. CONCLUSIONS

The results of the present study lead to the following conclusions:

1. Palladium migrates through the SiC coating without actually thinning this layer. The penetration appears to be linear with time at a rate represented by x/t ($\mu m/s$) = $0.0319 \exp(-128{,}000/RT)$ for $1500 \leq T \leq 1780$ K. The penetration characteristics are not inconsistent with a grain-boundary-diffusion mechanism.

2. Palladium–SiC interactions were prevented at $1670 \leq T \leq 1920$ K by doping kernels to form previously unknown U-Pd-Si-C compounds. A UO_2-UC_2-SiC kernel is preferred.

3. Rare-earth interaction with the SiC layer appears to be linear with time. This applies to the range $1500 \leq T \leq 1775$ K from the present study and the range $1575 \leq T \leq 2175$ K from a previous study.[1] Other studies[2,3,14] demonstrated that rare-earth attack is preventable by use of oxide or oxide-carbide kernels having the proper stoichiometry.

4. Silver–SiC interactions sufficient to determine the reaction time dependence could not be detected by the present techniques, nor was silver observed in the SiC by high-resolution microscopy.

5. The palladium and rare-earth interactions and their time dependence should be confirmed in-reactor, as should the proposed retention of palladium by SiC additions to UO_2-UC_2 kernels. In-reactor testing is particularly important because the palladium contamination of the SiC in the as-coated particles (except for the kernels with SiC additions) may affect the present rate data in an unknown manner (Sects. 2.1 and 2.3).

6. The effect of microstructural control of the SiC coating to reduce palladium migration is rather weak in comparison to the effects of temperature. Conclusion 2 indicates that Pd–SiC interactions might be eliminated altogether.

6. REFERENCES

1. R. L. Pearson and T. B. Lindemer, "The Interaction of LaC_2 and NdC_2 with SiC in HTGR Particles," in *Proc. of the Topical Meeting on Thermal Reactor Safety*, Vol. 3, CONF-770708 (held June 31–July 4, 1977, Sun Valley, Idaho), pp. 357-71.

2. F. J. Homan, T. B. Lindemer, E. L. Long, Jr., T. N. Tiegs, and R. L. Beatty, "Stoichiometric Effects on Performance of High-Temperature Gas-Cooled Reactor Fuels from the U-C-O System," *Nucl. Technol.* 35(2): 428-41 (September 1977).

3. R. L. Pearson and T. B. Lindemer, *Simulated Fission Product Oxide Behavior in Triso-Coated HTGR Fuel*, ORNL/TM-6741 (August 1979).

4. T. N. Tiegs, *Fission Product Pd–SiC Interaction in Irradiated Coated Particle Fuels*, ORNL/TM-7203 (April 1980).

5. R. J. Lauf, *The Interaction of Silver and Palladium with Silicon Carbide in HTGR Fuel Particles – Preliminary Report*, ORNL/TM-7393 (July 1980).

6. R. L. Pearson, T. B. Lindemer, and E. C. Beahm, *Simulated Fission Product–SiC Interaction in Triso-Coated LEU or MEU HTGR Fuel Particles*, ORNL/TM-6991 (November 1980).

7. J. C. d'Entremont and J. Chipman, "The Free Energy of Silicon Carbide from Its Solubility in Silver," *J. Phys. Chem.* 67: 499-501 (1963).

8. HTGR Generic Technology Program, *Semiannual Report for Period Ending March 31, 1980*, GAA-15842 (May 1980).

9. J. I. Federer, *Fluidized Bed Deposition and Evaluation of Silicon Carbide Coatings on Microspheres*, ORNL/TM-5152 (January 1977).

10. R. J. Lauf and D. N. Braski, *Dependence of Silicon Carbide Coating Properties on Deposition Parameters: Preliminary Report*, ORNL/TM-7209 (May 1980).

11. T. B. Lindemer and R. L. Pearson, "Kernel Migration for HTGR Fuels for the System Th-U-Pu-C-O-N," *J. Am. Ceram. Soc.* 60: 5-17 (1977).

12. P. Krautwasser, personal communication to R. L. Pearson, September 1981.

13. J. D. Honz, "Self-Diffusion of Carbon-14 and Silicon-30 in Alpha Silicon Carbide Single Crystal," Ph.D. Thesis, North Carolina State University at Raleigh, 1978.

14. T. N. Teigs, T. B. Lindemer, and T. J. Henson, "Fission Product Behavior in UC_xO_y Fissile Particles Made From Weak-Acid Resins," *J. Nucl. Mater.* 99: 222-234 (1981).

15. R. Ballestracci, "Crystal Structure of New Rare-Earth Compounds MRh_2Si_2 and MPd_2Si_2," *C. R. Acad. Sci. Paris B*, 282: 291-292 (1976).

16. Ref. 6, p. 4.

17. Ref. 6, pp. 59-61.

Table A-1. Thinning of SiC by palladium in Triso-coated particles[a]

Batch No.	Particle No.	Maximum penetration (μm)	$10^4/T$[b] (K^{-1})	Time (h)
Pd-1	1	10.0	5.640	485
Pd-1	2	8.5	5.822	485
Pd-1	3	9.3	5.776	485
Pd-1	4	5.9	5.870	485
Pd-1	5	9.3	6.190	485
Pd-1	6	9.3	6.226	485
Pd-1	7	7.4	6.262	485
Pd-1	8	10.0	5.968	485
Pd-1	9	4.1	6.567	995
Pd-1	10	7.0	6.648	995
Pd-1	11	2.6	6.689	995
Pd-1	12	9.6	6.567	995
Pd-1	13	5.9	6.411	995
Pd-1	14	5.2	6.317	995
Pd-1	15	14.8	6.190	995
Pd-1	16	7.4	6.051	995
Pd-1	17	7.4	6.068	995
Pd-1	18	15.2	6.001	995
Pd-1	19	12.6	6.085	995
Pd-1	20	12.6	5.984	995
Pd-1	21	11.1	5.935	995
Pd-1	22	13.0	5.700	995
Pd-1	23	14.1	5.761	995
Pd-1	24	12.2	5.715	995
Pd-2	25	2.6	6.392	995
Pd-2	26	9.3	5.968	995
Pd-2	27	8.1	5.886	995
Pd-2	28	23.3	5.854	995
Pd-2	29	19.3	5.625	995
Pd-2	30	25.9	5.640	995
Pd-2	31	18.1	5.670	995
Pd-2	32	15.2	5.761	995
Pd-2	33	27.8	5.919	2000
Pd-2	34	24.8	5.984	2000
Pd-2	35	27.0	5.968	2000
Pd-2	36	21.9	6.085	2000
Pd-2	37	18.1	6.103	2000
Pd-2	38	17.4	6.146	2000
Pd-2	39	27.8	6.226	2000
Pd-2	40	23.0	6.217	2000
Pd-2	41	10.4	6.271	2000
Pd-2	42	13.0	6.345	2000
Pd-2	43	8.9	6.449	2000
Pd-2	44	16.7	6.507	2000
Pd-2	45	7.4	6.627	2000
Pd-1	46	19.3	6.527	4016
Pd-1	47	10.4	6.689	4016
Pd-1	48	14.1	6.547	4016
Pd-2	49	27.4	6.354	4016
Pd-2	50	28.5	6.468	4016
Pd-2	51	22.2	6.430	4016
Pd-2	52	21.5	6.587	4016

[a] Data used to determine Eq. (2), Sect. 2.3.2 of text.

[b] T = temperature.

Table A-2. Thinning of SiC by palladium in Triso-coated particles over 2000 h[a]

Batch No.	Particle No.	T[b] (K)	$10^4/T$ (K^{-1})	Maximum penetration (μm)
Pd-1	7	1650	6.06	14.1
	9	1605	6.23	11.8
	10	1605	6.23	11.8
	12	1577	6.34	7.1
	13	1572	6.36	14.1
	16	1550	6.45	6.5
	17	1548	6.46	6.5
	18	1513	6.61	5.3
Pd-2	4	1701	5.88	12.6
	5	1689	5.92	27.8
	6	1672	5.98	24.8
	7	1675	5.97	27.0
	9	1642	6.09	21.9
	10	1639	6.10	18.1
	11	1629	6.14	17.4
	12	1605	6.23	27.8
	13	1608	6.22	23.0
	14	1595	6.27	10.4
	15	1577	6.34	13.0
	17	1550	6.45	8.9
	19	1536	6.51	16.7
	21	1508	6.63	7.4
Pd-6	1	1560	6.41	15.28
	4	1587	6.30	18.18
	5	1577	6.34	18.18
	6	1577	6.34	17.27
	7	1605	6.23	20.19
	10	1634	6.12	30.00
	14	1675	5.97	40.91
Pd-8	1	1592	6.28	5.45
	3	1587	6.30	18.18
	5	1621	6.17	10.00
	8	1653	6.05	14.55
	11	1684	5.94	15.45

Table A-2 (continued)

Batch No.	Particle No.	T[b] (K)	$10^4/T$ (K^{-1})	Maximum penetration (μm)
Pd-10	2	1684	5.94	10.90
	7	1610	6.21	5.45
	8	1645	6.08	16.36
	9	1669	5.99	11.82
	10	1639	6.10	25.45
	11	1621	6.17	24.55
	12	1600	6.25	42.73
	13	1587	6.30	18.18
	17	1603	6.24	17.27
Pd-11	3	1701	5.88	7.27
	4	1675	5.97	8.18
	8	1582	6.32	18.18
	9	1605	6.23	10.00
	11	1621	6.17	6.36
	16	1575	6.35	10.90
	17	1597	6.26	11.82
	18	1587	6.30	13.64
Pd-12	3	1678	5.96	9.09
	6	1634	6.12	13.64
	9	1570	6.37	10.00
	10	1550	6.45	8.18
	11	1531	6.53	9.09
	12	1555	6.43	9.09
	13	1575	6.35	20.00
	14	1585	6.31	8.18
	15	1603	6.24	7.27
	16	1629	6.14	11.82

[a]For study of SiC deposition temperature effects on palladium interactions with SiC (Sect. 3.1).

[b]T = temperature.